Structural, Morphological and Electrical Properties of SiC:PVA:PEDOT:PSS Paper-Based Materials for Flexible Strain Sensors

Burak Y. Kadem

College of Science,
Al-Karkh University of Science,
Baghdad, IRAQ

In this study, we investigated the impact of acidic composite solutions on cellulose structures and evaluated the morphology, structural properties, and electrical performance of SiC:PVA:PEDOT:PSS composites. Optical microscopy revealed that acidic solutions significantly damage cellulose, whereas incorporating PVA prevents such damage, creating a rod-like structure beneficial for sensor applications. X-ray diffraction (XRD) analysis showed a transition from amorphous to crystalline phases in samples treated with H_2SO_4, highlighting improved crystallinity. Fourier-transform infrared (FTIR) spectroscopy indicated enhanced intermolecular hydrogen bonding and conformational changes within the polymer matrix, contributing to increased electrical conductivity. Scanning electron microscope (SEM) images illustrated varying morphologies influenced by acid treatments, with PEDOT:PSS and PVA forming smooth, compact structures. Electrical measurements demonstrated a substantial rise in conductivity and decreased sheet resistance, with the highest conductivity observed in samples treated with H_2SO_4. The composites were successfully tested as strain sensors, showing promising performance in response to human actions, underscoring their potential for practical applications.

Keywords: Silicon carbide; Cellulose; Polymer electrolyte; Paper strain sensor
Received: 30 November 2024; **Revised:** 1 May 2025; **Accepted:** 8 May 2025

1. Introduction

Cellulose-rich paper-based devices have attracted growing interest due to their flexibility, affordability, environmental friendliness, simple fabrication methods, biocompatibility, porosity, and high surface-volume ratio, making them suitable for various flexible electronic applications [1-3]. Conductive polymers, which have promising properties for sensor fabrication, include simple processing methods, high conductivity, and biocompatibility. Among these, poly(3,4-ethylenedioxythiophene) doped with poly(styrene sulfonate) (PEDOT:PSS) stands out due to its soft nature, combined electronic and ionic conductivity, and printability [4]. PEDOT:PSS is well-suited for deposition onto inexpensive and eco-friendly paper substrates, offering an excellent opportunity for creating disposable, environmentally-friendly flexible electronics [5,6]. PEDOT:PSS consists of insulating PSS domains that restrict charge transport between conjugated PEDOT domains by increasing the π–π stacking distance [7,8]. As PEDOT:PSS is a conductive polymer, increasing its conductivity is essential, which can be achieved by separating the PSS domains from the PEDOT domains using several methods such as acid treatment [9-11]. The long PSS chains compel the shorter PEDOT chains to adopt a coiled structure, resulting in poor inter-grain connections between PEDOT lamellae [12]. During acid treatment, the acid dissociates into cations and anions, targeting the positively charged PEDOT and the negatively charged PSS, disrupting their ionic interactions, leading to their separation and allowing for selective removal of PSS from the system [13]. By removing the PSS, the π–π stacking distance decreases, causing the PEDOT grains to change from a coiled to a fibrillary conformation. In this new structure, a dense PEDOT network aligns along the edge-on direction [14]. Consequently, reducing the π–π stacking distance and improving the interconnection between PEDOT grains facilitates the mobility of charge carriers [15]. Several efforts to fabricate flexible PEDOT:PSS using cellulose as building blocks have been carried out. For instance, Ko et al. [16] demonstrated the preparation of highly conductive PEDOT:PSS/cellulose nanofiber nano paper through vacuum filtration. Wang and co-authors [17] reported the use of solution-based reactions to fabricate PEDOT nano paper used as electrodes for symmetric supercapacitors. Poly (vinyl alcohol) (PVA) hydrogels are widely used due to their low cost, good mechanical properties, high water content, and good biocompatibility [18,19]. PVA has been extensively used in wearable sensors [20], soft actuators [21], and soft strain sensors matrices [22]. Flexible strain sensors are mostly prepared by combining functional conductive materials with elastic polymers [23,24]. Pressure and strain sensors have gathered significant attention among various sensor technologies due to their potential applications in next-generation human health monitoring, such as

motion detection, machine interaction, soft robotics, and electronic skin [25,26]. In general, pressure and strain sensors convert external stimuli into electrical signals such as resistance, current, capacitance, and voltage. These stimuli can be either tensile forces or pressure, and in both scenarios, the sensor is composed of electrodes and sensing elements. Pressure and strain sensors are classified based on their working principles, which include piezoelectric, piezoresistive, and capacitive sensors. Among these, piezoresistive wearable sensors have attracted significant attention due to their simple structure, straightforward sensing mechanism, and low cost [27]. To demonstrate piezoresistive properties, wearable resistive pressure and strain sensors should incorporate compressible, flexible, and/or stretchable substrates along with electrically conductive materials. Additionally, they must possess high sensitivity, rapid response, a wide detection range, skin compatibility, biocompatibility, and durability over multiple detection cycles [28]. Silicone rubber polymers like polydimethylsiloxane (PDMS) have been extensively used as substrates for pressure and strain sensors due to their flexibility and stretchability [29]. However, these materials do not meet all the necessary criteria, such as skin compatibility and the potential for production from renewable raw materials. As a result, cellulosic materials, particularly nanocellulose, have emerged as a promising candidate for developing such sensors. They offer exceptional properties including skin compatibility, low-cost production, non-toxicity, renewability, biodegradability, and flexibility [30]. Additionally, these materials offer a significant opportunity to create substrates with high mechanical strength, large surface area, high aspect ratio, and, most importantly, a wide range of customizability due to the potential for hydroxyl group modifications [31]. However, nanocellulose materials need to be optimized to meet the specific requirements of pressure and strain sensors. For example, they typically exhibit low electrical conductivity, and some structures have low resistance to compression or stretching. To address these challenges, researchers have explored composites and 3D structures to develop high-performance sensors. It is important to note that the inherent tunability of mechanical properties is highly advantageous for creating sensors with various sensitivity ranges. For example, highly sensitive sensors can detect weak pressing or tensile forces. Additionally, 3D structures are extremely beneficial for sensor design, as they allow the incorporation of additives or blending materials, enhancing electrical properties and enabling multiple responses. Another approach involves combining nanocellulose with other polymers to create bio-composites. Generally, these bio-composites are designed to enhance resistance to compression and tension. The literature provides examples of bio-composites made from CNC and CNF with polymeric matrices like PDMS, waterborne polyurethane, alginate, and PVA [32]. Typically, this incorporation occurs by infiltrating the desired polymer into the cellulosic porous materials, resulting in improved mechanical properties [22]. On the other hand, SiC has over 200 crystal structures known as polytypes, with most research focusing on 3C-, 4H-, and 6H-SiC. The 4H- and 6H- polytypes are preferred for piezoresistive devices due to their excellent properties, including higher energy band gaps (3.2 eV for 4H and 3.0 eV for 6H) compared to 3C (2.3 eV). This high potential barrier minimizes electron-hole pairs at high temperatures, ensuring the stability of SiC electronic devices and sensors [33-35]. The change in resistance results from two factors: modifications in the resistor's dimensions and geometry, and variations in the material's resistivity. A material's piezoresistance is influenced by several factors, including chemical composition, crystal structure (polytype), crystal orientation, and the type and concentration of dopants [36].

In the current study, several approaches were developed: first, the preparation of SiC powder at low temperatures using a simple method; secondly, the use of PEDOT:PSS in two forms, as a solution and as pellets. Doping PEDOT:PSS with acids, whether starting with pellets or solution, introduces conductivity enhancements and structural changes. However, the choice between using pellets or solution PEDOT:PSS can significantly affect the doping process and final properties due to differences in how the doping is carried out and the state of the material. For high-performance applications requiring optimized doping (e.g., flexible electronics or high-conductivity films), pellets may be preferred. For routine or large-scale production, solutions are often more practical. The main idea of using PEDOT:PSS pellet to compare with solution PEDOT:PSS is to and finally, the new electrolyte based on SiC:PVA:PEDOT:PSS. To the best of the authors' knowledge, this is the first attempt to fabricate a strain sensor based on this electrolyte.

2. Experimental Part

PEDOT:PSS 3.0-4.0% in H_2O, high-conductivity grade solution, dry re-dispersible PEDOT:PSS pellets, hydrochloric acid (HCl), sulfuric acid (H_2SO_4), and PVA M_w ($8.9x10^4$-$9.8x10^4$), 99+% hydrolyzed were purchased from Sigma Aldrich. Furthermore, carbon black powder was purchased from Arihant Chemical-India (95%), while silicon powder, 325 mesh (99%) trace metals basis was purchased from Ottokemi Pvt. Ltd.

PVA powder (5g) was dissolved in 100 mL of deionized (DI) water using a pre-cleaned container. A viscous solution was obtained after 45 minutes of vigorous stirring on a hot plate at 70°C until the

solution became homogeneous, and then it was cooled down to room temperature to be ready for further use.

Silicon powder (1 g) and carbon black powder (1 g) were dissolved in 35 mL of H_2SO_4 acid under stirring at room temperature, separately. The ratio of the Si to C is considered based on the literature [37]. The Si based and C based solutions were mixed and the resultant solution was stirred for 5 hours in a round bottom flask. The resultant solution was kept in dark overnight for further use.

PEDOT:PSS pellets (40 mg) dissolved in 20 mL of H_2SO_4 and another 40 mg of these pellets dissolved in 20 mL HCl under the same ambient conditions. The solutions were kept under continuous stirring for an hour until a thick homogenous black liquid was obtained. On the other hand, 40 mL of PEDOT:PSS solution was doped in 20 mL of H_2SO_4 and 20 mL of HCl, separately, to alter the surface morphology and electrical properties and for comparison. This process occurred under continuous stirring for one hour to prevent aggregation of PEDOT:PSS at room temperature.

The final gel electrolyte solution (GES) was prepared by mixing PVA, SiC, PEDOT:PSS solution in the volume ratio of (1:1:1) under stirring at room temperature for 1 hour. The final samples are as follows: SiC:PVA (Pure) sample, SiC:PEDOT:PSS (powder doped with HCl) is (S1) sample, SiC:PEDOT:PSS (Liquid doped with HCl) is (S2) sample, SiC:PEDOT:PSS (Liquid doped with H_2SO_4) is (S3) sample and SiC:PEDOT:PSS (powder doped with H_2SO_4) is (S4) sample.

The paper-based strain sensor was prepared by soaking a sheet of cellulose paper in the GES and this paper was kept in Petri dish covered overnight. Then two electrodes based on Cu tape and Al tape was used.

3. Results and Discussion

As the composite solutions are acid-based, this has a significant impact on the cellulose structure. Therefore, an investigation of the morphology of the studied composites deposited on a cellulose paper was carried out using an optical microscope as shown in Fig. (1). When acidic solutions are deposited on the cellulose paper, clear damage is observed as shown in Fig. (1A-E). The presence of the acid has a direct impact on the cellulose microstructure. However, using PVA as shown in Fig. (1F-J) prevents any possible damage to the cellulose structure [37]. The latter structure contains aggregates of nanocrystallites joined together by local lateral crystalline structure and forming a rod like structure as predicted by the optical images. This morphology can boost the penetration and diffusion of moisture resulting in efficient sensor application [38]. In general, using PVA with the composite assists in the cellulose structure.

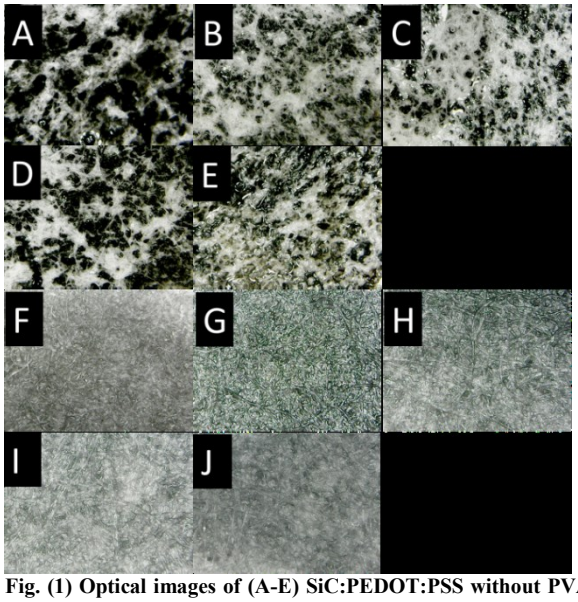

Fig. (1) Optical images of (A-E) SiC:PEDOT:PSS without PVA (Pure, S1, S2, S3 and S4, respectively) and (F-J) SiC:PEDOT:PSS:PVA (Pure, S1, S2, S3 and S4, respectively)

XRD was carried out to evaluate the structural properties of the samples. The peak positions, full-width at half maximum (FWHM) and d-spacing were estimated by X'pert High Score plus program. The average crystallite size was evaluated using Scherer's equation [39]:

$$D = \frac{k\lambda}{\beta cos\theta} \quad (1)$$

where D is the crystalline size, λ is the wavelength of the radiation, k is called Scherrer's constant, β is the FWHM and θ is the diffraction peak position

It is well-known that cellulose is a natural polymer consisting of linear chain based on van der Waals and intermolecular hydrogen bonds between hydroxyl groups and oxygen [40]. Therefore, cellulose chains may aggregate, forming a crystalline micro-fibrils region which consists of highly ordered cellulose molecules and/or micro-fibrils amorphous region [41]. The XRD results of the samples are illustrated in Fig. (2A) and the corresponding parameters are shown in table (1). The pure and S1 samples have amorphous structures and no crystalline region is observed. This amorphous structure is attributed to the cellulose structure (see Fig. 2B) in both pure and S1 sample, and further attributed to the rich-PSS domains located at the upper layer in S1 sample [42]. This amorphous structure is enhanced in S2, S3 and S4 samples showing crystalline regions. The peak's intensity has increased gradually for all other samples, indicating a change from the amorphous phase to the crystalline phase. In S2 sample, the very small diffraction peaks at around 2θ of 12° are attributed to the lamellar stacking distance of the molecular structure of PEDOT and PSS [42]. Mainly, both PVA and PEDOT:PSS are semi-crystalline polymers, therefore, the interaction between them with the addition of

secondary dopants influences their crystallinity [43]. Doping SiC:PVA with PEDOT:PSS treated with H_2SO_4 in both cases as powder and liquid results in further improvement in the crystal structure. In case of S3 sample, strong peaks around 2θ of 12°, 14.9°, 16.5°, 22.6° and 23.1° are observed. In S4 sample, the diffraction peak around 2θ of 12° is disappears, while the diffraction peak around 14.9° (in S3) has shifted to 15.5° (in S4) and the diffraction peak at around 16.5° (in S3) has shifted to 16.3° (in S4) and the diffraction peaks at 22.6° and 23.1° (in S3) are combined together in one diffraction peak at 22.9° (in S4). The H_2SO_4 treatment induces the crystalline structure and affects the arrangement of the PEDOT chain through sulfuric acid and the removal of amorphous PSS [44].

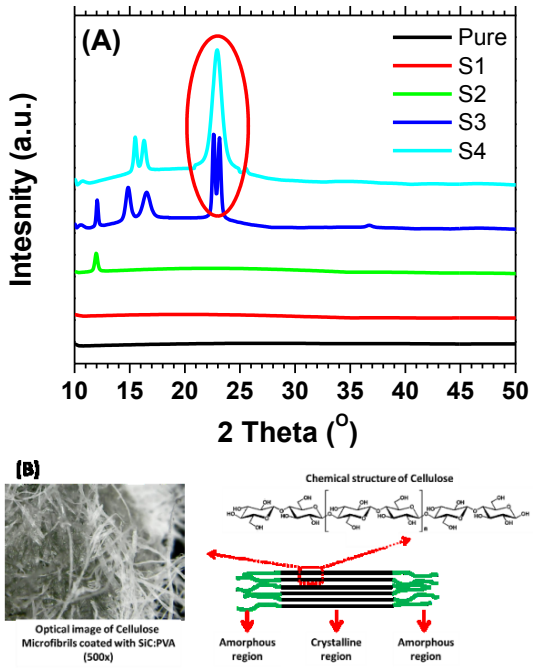

Fig. (2) (A) XRD spectra of SiC:PVA :PEDOT:PSS as liquid and powder form and (B) the cellulose microfibrils and structure with an optical image of cellulose

Table (1) XRD parameters of SiC:PVA:PEDOT:PSS composites

Sample	Position [2θ] (deg)	d-spacing (nm)	FWHM (deg)	D (nm)
Pure	-	-	-	-
S1	-	-	-	-
S2	12	0.738	0.3	27.8
S3	12	0.735	0.197	42.4
	14.9	0.597	0.492	17.0
	16.5	0.537	0.787	10.7
	22.6	0.393	0.246	34.4
	23.1	0.385	0.295	28.7
S4	15.5	0.572	0.295	28.4
	16.3	0.544	0.394	21.3
	22.9	0.388	0.984	8.6

Fourier-transform infrared spectroscopy (FTIR) was used to evaluate the functional groups of the composites and investigate the formation of the crosslinking network from the blends of SiC:PVA and PEDOT:PSS.

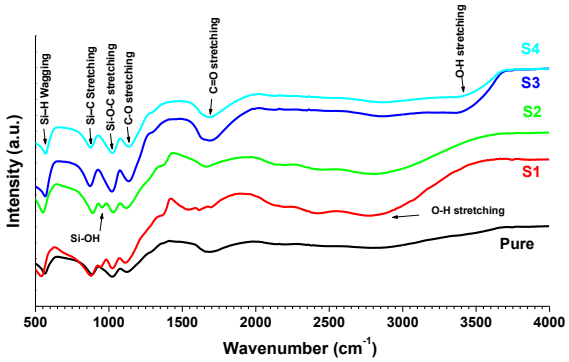

Fig. (3) FTIR spectra of SiC:PVA:PEDOT:PSS

The FTIR spectra are shown in Fig. (3) and the FTIR parameters are presented in table (2). Hydroxyl group (-OH) related to the cellulose structure is observed in the range of around 2900 cm^{-1} in pure sample and it becomes more pronounced in S1 and S2 samples. This indicates higher intermolecular hydrogen bonding (H-bonds). This peak has shifted towards a higher wavenumber in S3 and S4 samples to be in around 3400 cm^{-1}. The reason for such a shift could be attributed to an alteration in the strain [45]; H-bonds can support the polymeric composite with extraordinary mechanical properties [46,47].

Table (2) The IR transmission bands of powder SiC films and their assignments

Position (cm^{-1})	Vibration Mode	Possible Origin	Ref
560	Si–H Wagging	SiC backbone (common in Si-based compounds).	[50]
880	Si–C Stretching	Characteristic of SiC materials.	[51]
960	Si–OH	Surface hydroxylation of SiC or Si-based materials.	[48]
1080	Si–O–C Stretching	Indicates bonding between SiC and organic/inorganic components.	[52]
1150	C–O Stretching	PEDOT:PSS or organic compounds in PVA or dopants.	[53]
1700	C=O Stretching	PVA, PEDOT:PSS, or possible carboxylic acid groups.	[52]
2900	O–H Stretching	Aliphatic O-H, water content, or PVA interactions.	[54]
3400	O–H Stretching	Broad hydroxyl peak (from adsorbed water or acid dopants).	[54]

Peaks around 1700 cm^{-1} are ascribed to the C=O stretching of the carbon backbone and peaks around 1150 cm^{-1} are attributed to the stretching vibrations of C–O and C–O–C groups of PVA matrix. Additionally, peaks around 1000-1080 cm^{-1} are attributed to the Si-O-C stretching of the SiC particles. A peak around 960 cm^{-1} is observed in S1 and S2 samples and is related to the vibration of Si-OH [48]. When SiC:PVA is embedded into PEDOT:PSS chains, it results in conformational changes in the polymer backbone from

coiled to linear structures [49]; this may increase the electrical conductivity by creating charge pathways through this network. Peaks around 880 cm^{-1} are ascribed to the Si–C Stretching vibration mode of the SiC particles while peaks around 560 cm^{-1} are assigned to the Si–H wagging vibration mode of the SiC particles. This peak is shifted when the PEDOT:PSS doped with HCl is used (for both liquid and powder PEDOT:PSS) indicating π-π interactions between PEDOT:PSS and SiC nanoparticles.

The morphology of the prepared composites was investigated using a SEM and the results are shown in Fig. (4). SiC clusters were observed in the pure sample which might result from the aggregation of SiC nanoparticles distributed within the PVA polymer matrix; this results in good agreement with the literature [55]. In the S1 sample, flake-like shapes are observed when PEDOT:PSS treated with HCl acids (for both liquid and powder PEDOT:PSS) is used. However, these features are more pronounced in the S2 samples. The HCl treatment and the use of pellet PEDOT:PSS influence SiC:PVA structure and result in different morphology. Such change is mainly attributed to the separation of PEDOT from PSS chains by this acid treatment [11]. The presence of the acidic PEDOT:PSS domains around SiC:PVA domains led to a smooth, flat, and compact morphology of the SiC:PVA:PEDOT:PSS (S1 sample). Furthermore, treating pellet PEDOT:PSS with H_2SO_4 (S3 sample) results in similar, smaller and compact flake-like features covered by very fine ribbon features whereas the S4 sample results in similar features with the absence of these ribbon features.

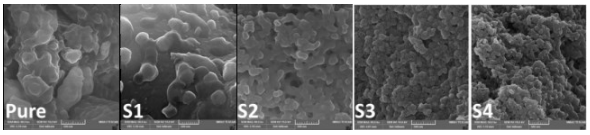

Fig. (4) SEM images of the SiC:PVA:PEDOT:PSS samples treated with different acids

The electrical conductivity and sheet resistance of the paper based devices were characterized using IV measurements, and the results are demonstrated in Fig. (5A). Sheet of cellulose papers doped with SiC:PVA:PEDOT:PSS composites with the dimensions of (1×1×0.1cm) were used. The conductivity (σ) of the samples is calculated using the following equation [56]:

$$R = \frac{t}{A}\rho \qquad (2)$$

where t is the thickness, A is the area and ρ is the resistivity which is equal to inverse of conductivity (1/σ)

SiC:PVA (pure sample) has an electrical conductivity of 5.25 $S.cm^{-1}$. This has increased to 15.53 $S.cm^{-1}$ when PEDOT:PSS pellets were treated with HCl (S1 sample) while treating PEDOT:PSS solution with HCl (S2 sample) resulted in conductivity of 22.89 $S.cm^{-1}$. Moreover, using pellets of PEDOT:PSS treated with H_2SO_4 (S3 sample) resulted in higher electrical conductivity of 39.9 $S.cm^{-1}$ compare to other samples whereas S4 sample resulted in electrical conductivity of 34 $S.cm^{-1}$. This sharp increase in the electrical conductivity is attributed to the formation of the percolation network with the cellulose structure [54]. Such enhancement results in decreasing the sheet resistance of these samples.

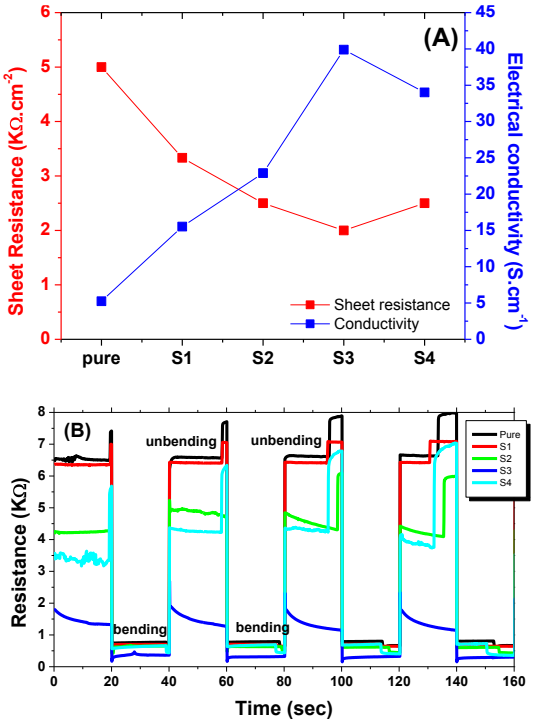

Fig. (5) (A) Electrical conductivity and sheet resistance of the paper based sample, (B) time dependence of the paper based sensor and (C) strain sensor under test

The samples were examined as strain paper sensor in response to human actions where these paper based samples were sandwiched between two electrodes (Cu and Al); results in Fig. (5B) show time dependence results of these sensors, the time interval for pressing is 20 s and the recovery time is 20 s. The paper based sensor is engineered to use cellulose to act as high surface-area electrodes to improve conductivity [57]. The fabricated strain sensor was fixed onto an index finger and recorded the response during the bending

and unbending actions as shown in Fig. (5C). When the strain sensor is bent, the paper substrate undergoes physical deformation; when the PEDOT:PSS is exposed to an elongation then PEDOT and PSS align themselves according to the stress direction to be more stable in where PEDOT:PSS is considered as a piezoelectric material, consequently, a change in the electrical resistance occurs. Generally, sensor response results from both the geometrical effect and a change in the percolation network system due to the reorganization of their internal structure during elongation [58].

4. Conclusion

The study demonstrates the successful fabrication and evaluation of a paper-based strain sensor using SiC:PVA:PEDOT:PSS electrolyte composites. By employing PEDOT:PSS in pellet and solution forms and treating it with HCl and H_2SO_4, the electrolyte properties were effectively modified. While acidic solutions damaged the cellulose structure, the inclusion of PVA prevented this damage and promoted the formation of beneficial rod-like structures. The crystallinity was enhanced in samples treated with H_2SO_4 compared to those treated with HCl. The presence of functional groups and crosslinking networks was confirmed, with shifts in the O-H stretching bands indicating improved mechanical properties. Distinct morphological differences influenced by acid treatment and PEDOT:PSS form were displayed. Significant variations were shown with the highest conductivity observed in the sample treated with H_2SO_4 and PEDOT:PSS pellets (S3). This improvement was linked to a percolation network within the cellulose structure, reducing sheet resistance. The strain sensors demonstrated good sensitivity to bending and unbending actions, highlighting their practical application potential. Overall, the study successfully enhanced the structural, morphological, and electrical properties of paper-based strain sensors, paving the way for cost-effective and efficient sensor applications.

References

[1] K. Kim et al., "Based printed circuit boards", *in 2015 15th Int. Conf. on Control, Automation and Systems (ICCAS), IEEE,* 13 October 2015, pp. 1857-1859.

[2] A.W. Martinez et al., "Patterned paper as a platform for inexpensive, low- volume, portable bioassays", *Angewandte Chemie,* 119(8) (2007) 1340-1342.

[3] Y. Lin et al., "Recent advancements in functionalized paper-based electronics", *ACS Appl. Mater. Interfaces,* 8(32) (2016) 20501-20515.

[4] S. Inal et al., "Conjugated polymers in bioelectronics", *Accounts Chem. Res*., 51(6) (2018) 1368-1376.

[5] S. Sakkopoulos and E. Vitoratos, "'Differentiation of the aging process of PEDOT:PSS films under inert Helium and ambient atmosphere for two different rates of thermal treatment", *Open J. Org. Polym. Mater.,* 4(1) (2014) 1-5.

[6] D. Nilsson et al., "An all-organic sensor–transistor based on a novel electrochemical transducer concept printed electrochemical sensors on paper", *Sens. Actuat. B: Chem*., 86(2-3) (2002) 193-197.

[7] K. Itoh et al., "Structural alternation correlated to the conductivity enhancement of PEDOT: PSS films by secondary doping", *The J. Phys. Chem. C*, 123(22) (2019) 13467-13471.

[8] S. Khasim et al., "Post treated PEDOT-PSS films with excellent conductivity and optical properties as multifunctional flexible electrodes for possible optoelectronic and energy storage applications", *Opt. Mater.,* 125 (2022) 112109.

[9] L. Bießmann et al., "Highly conducting, transparent PEDOT:PSS polymer electrodes from post- treatment with weak and strong acids", *Adv. Electron. Mater.,* 5(2) (2019) 1800654.

[10] W. Meng et al., "Conductivity enhancement of PEDOT: PSS films via phosphoric acid treatment for flexible all-plastic solar cells", *ACS Appl. Mater. Interfaces,* 7(25) (2015) 14089-14094.

[11] B.Y. Kadem et al., "The effects of the PEDOT: PSS acidity on the performance and stability of P3HT:PCBM-based OSCs", *J. Mater. Sci.: Mater. Electron.,* 29 (2018) 19287-19295.

[12] C. Greco et al., "Generic model for lamellar self-assembly in conjugated polymers: linking mesoscopic morphology and charge transport in P3HT", *Macromol.,* 52(3) (2019) 968-981.

[13] Z. Zhu et al., "Effective treatment methods on PEDOT:PSS to enhance its thermoelectric performance", *Synth. Met.*, 225 (2017) 31-40.

[14] M. Vosgueritchian, D.J. Lipomi and Z. Bao, "Highly conductive and transparent PEDOT:PSS films with a fluorosurfactant for stretchable and flexible transparent electrodes", *Adv. Func. Mater.,* 22(2) (2012) 421-428.

[15] E. Hosseini, V.O. Kollath and K. Karan, "The key mechanism of conductivity in PEDOT:PSS thin films exposed by anomalous conduction behaviour upon solvent-doping and sulfuric acid post-treatment", *J. Mater. Chem. C*, 8(12) (2020) 3982-3990.

[16] Y. Ko et al., "Fabrication of highly conductive porous cellulose/PEDOT:PSS nanocomposite

paper via post-treatment", *Nanomater.*, 9(4) (2019) 612.
[17] Z. Wang et al., "Solution-processed poly (3, 4-ethylenedioxythiophene) nanocomposite paper electrodes for high-capacitance flexible supercapacitors", *J. Mater. Chem. A*, 4(5) (2016) 1714-1722.
[18] F. Martínez-Gómez et al., "*in vitro* release of metformin hydrochloride from sodium alginate/polyvinyl alcohol hydrogels", *Carbohyd. Polym.*, 155 (2017) 182-191.
[19] M. Guo et al., "Silver nanoparticles/ polydopamine coated polyvinyl alcohol sponge as an effective and recyclable catalyst for reduction of 4-nitrophenol", *Mater. Chem. Phys.,* 225 (2019) 42-49.
[20] X. Jing et al., "Highly transparent, stretchable, and rapid self-healing polyvinyl alcohol/cellulose nanofibril hydrogel sensors for sensitive pressure sensing and human motion detection", *Sens. Actuat. B: Chem.*, 295 (2019) 159-167.
[21] Q. Chen et al., "Programmable polymer actuators perform continuous helical motions driven by moisture", *ACS Appl. Mater. Interfaces*, 11(22) (2019) 20473-20481.
[22] O.Y. Kweon et al., "Stretchable and self-healable conductive hydrogels for wearable multimodal touch sensors with thermoresponsive behavior", *ACS Appl. Mater. Interfaces*, 11(29) (2019) 26134-26143.
[23] N. Qaiser et al., "A robust wearable point- of-care CNT-based strain sensor for wirelessly monitoring throat-related illnesses", *Adv. Func. Mater.*, 31(29) (2021) 2103375.
[24] Y. He et al., "Wearable strain sensors based on a porous polydimethylsiloxane hybrid with carbon nanotubes and graphene", *ACS Appl. Mater. Interfaces,* 13(13) (2021) 15572-15583.
[25] L. Duan, D.R. D'hooge and L. Cardon, "Recent progress on flexible and stretchable piezoresistive strain sensors: From design to application", *Prog. Mater. Sci.*, 114 (2020) 100617.
[26] X. Wang et al., "Research progress of flexible wearable pressure sensors", *Sens. Actuat. A: Phys.,* 330 (2021) 112838.
[27] X. Wang, L. Zheng and T. Zhang, "Flexible sensing electronics for wearable/attachable health monitoring", *Small*, 13(25) (2017) 1602790.
[28] H. Nesser and G. Lubineau, "Strain sensing by electrical capacitive variation: From stretchable materials to electronic interfaces", *Adv. Electron. Mater.*, 7(10) (2021) 2100190.
[29] J. Chen et al., "Polydimethylsiloxane (PDMS)-based flexible resistive strain sensors for wearable applications", *Appl. Sci.,* 8(3) (2018) 345.
[30] Y. Gao et al., "Flexible and sensitive piezoresistive electronic skin based on TOCN/PPy hydrogel films", *J. Appl. Polym. Sci.,* 138(48) (2021) 51367.
[31] Q. Fu et al., "Emerging cellulose-derived materials: a promising platform for the design of flexible wearable sensors toward health and environment monitoring", *Mater. Chem. Front.,* 5(5) (2021) 2051-2091.
[32] K.B. Teodoro et al., "A review on the role and performance of cellulose nanomaterials in sensors", *ACS Sensors,* 6(7) (2021) 2473-2496.
[33] T. Kimoto and J.A. Cooper, **"Fundamentals of silicon carbide technology: growth, characterization, devices and applications",** John Wiley & Sons, (NJ, 2014).
[34] N.G. Wright, A.B. Horsfall and K. Vassilevski, "Prospects for SiC electronics and sensors", *Mater. Today,* 11(1-2) (2008) 16-21.
[35] L. Jiang and R. Cheung, "A review of silicon carbide development in MEMS applications", *Int. J. Comput. Mater. Sci. Surf. Eng.*, 2(3-4) (2009) 227-242.
[36] T. Wejrzanowski et al., "Design of SiC-doped piezoresistive pressure sensor for high-temperature applications", *Sensors,* 21(18) (2021) 6066.
[37] R.A. Hadhy and B.Y. Kadem, "Gel polymer electrolyte based on SiC:PVA composites for body motion sensor and paper based application", *in 2019 12th Int. Conf. on Develop. in eSystems Eng. (DeSE), IEEE,* 7 October 2019, pp. 730-735.
[38] T. Li et al., "Porous ionic membrane based flexible humidity sensor and its multifunctional applications", *Adv. Sci.*, 4(5) (2017) 1600404.
[39] B.Y. Kadem, M.K. Al-hashimi and A.K. Hassan, "The effect of solution processing on the power conversion efficiency of P3HT-based organic solar cells", *Energy Procedia,* 50 (2014) 237-245.
[40] M.K.D. Rambo and M. Ferreira, "Determination of cellulose crystallinity of banana residues using near infrared spectroscopy and multivariate analysis", *J. Brazilian Chem. Soc.,* 26 (2015) 1491-1499.
[41] R.J. Moon et al., "Cellulose nanomaterials review: structure, properties and nanocomposites", *Chem. Soc. Rev.,* 40(7) (2011) 3941-3994.
[42] Y. Kim, Y. Kim and J.H. Kim, "Highly conductive PEDOT:PSS thin films with two-dimensional lamellar stacked multi-layers", *Nanomater.*, 10(11) (2020) 2211.
[43] D.A.A. Ruzaidi et al., "Revealing the improved sensitivity of PEDOT:PSS/PVA thin films

through secondary doping and their strain sensors application", *RSC Adv.,* 13(12) (2023) 8202-8219.

[44] N. Kim et al., "Highly conductive PEDOT:PSS nanofibrils induced by solution- processed crystallization", *Adv. Mater.*, 26(14) (2014) 2268-2272.

[45] T. Liu et al., "Hydrogen- bonded polymer–small molecule complexes with tunable mechanical properties", *Macromol. Rapid Commun.,* 39(9) (2018) 1800050.

[46] G. Song et al., "Facile fabrication of tough hydrogels physically cross-linked by strong cooperative hydrogen bonding", *Macromol.,* 46(18) (2013) 7423-7435.

[47] G. Song et al., "Rheological behavior of tough PVP-*in situ*-PAAm hydrogels physically cross-linked by cooperative hydrogen bonding", *Macromol.,* 49(21) (2016) 8265-8273.

[48] K. Fu et al., "Nano-Cavities within Nano-Zeolites: The Influencing Factors of the Fabricating Process on Their Catalytic Activities", *Nanomater*., 13(13) (2023) 1923.

[49] Y. Seekaew et al., "Low-cost and flexible printed graphene–PEDOT:PSS gas sensor for ammonia detection", *Org. Electron.,* 15(11) (2014) 2971-2981.

[50] T. Shariatmadar et al., "Pressure dependent structural and optical properties of silicon carbide thin films deposited by hot wire chemical vapor deposition from pure silane and methane gases", *J. Mater. Sci.: Mater. Electron.,* 24 (2013) 1361-1368.

[51] T. Kaneko et al., "FTIR analysis of a-SiC: H films grown by plasma enhanced CVD", *J. Cryst. Growth,* 275(1-2) (2005) e1097-e1101.

[52] H.S. Mohsen and H.M.A. Hasan, "Optical Properties of PVA Silicon Carbide Nano Composites Films Synthesized Via Laser Ablation", *J. Univ. Babylon Pure Appl. Sci.,* (2023) 123-136.

[53] S. Mahendia et al., "Optical and structural properties of poly (vinyl alcohol) films embedded with citrate-stabilized gold nanoparticles", *J. Phys. D: Appl. Phys.,* 44(20) (2011) 205105.

[54] Y.F. Zhang et al., "Flexible, stretchable and conductive PVA/PEDOT:PSS composite hydrogels prepared by SIPN strategy", *Polym. Test.,* 81 (2020) 106213.

[55] Z. An et al., "A facile synthesis of silicon carbide nanoparticles with high specific surface area by using corn cob", *Adv. Powder Technol.,* 30(1) (2019) 164-169.

[56] B. Kadem, W. Cranton and A. Hassan, "Metal salt modified PEDOT:PSS as anode buffer layer and its effect on power conversion efficiency of organic solar cells", *Org. Electron.,* 24 (2015) 73-79.

[57] V.L. Pushparaj et al., "Flexible energy storage devices based on nanocomposite paper", *Proc. Nation. Acad. Sci.,* 104(34) (2007) 13574-13577.

[58] A. Hu et al., "Crystallization and conformation engineering of solution-processed polymer transparent electrodes with high conductivity", *J. Mater. Chem. C,* 5(2) (2017) 382-389.

